Molecular structure and electron density distribution in the crystals of 3,6-dimethoxy-1,2,4,5-tetrazine and 3-phenyl-1,2,4,5-tetrazine based on X-ray diffraction data at 120 and 150 K. "Bent" bonds in the six-membered heterocycle

M. Yu. Antipin,[a]* T. V. Timofeeva,[a] D. S. Yufit,[a] and J. Sauer[b]

*[a]Institute of Organoelement Compounds, Russian Academy of Sciences,
28 ul. Vavilova, 117813 Moscow, Russian Federation.
Fax: +7 (095) 135 5085*
*[b]Institute of Organic Chemistry, University of Regensburg,
93053 Regensburg, Germany.
Fax: 49 (941) 943 4946*

Characteristic features of the molecular geometry and electron density distribution in the crystals of 3,6-dimethoxy-1,2,4,5-tetrazine and 3-phenyl-1,2,4,5-tetrazine have been studied by X-ray structural analysis and quantum-chemical (RHF and MP2) and molecular mechanics (MM3) calculations. An unusual shift of the maxima of the deformation electron density from the N—N bonds toward the center of the heterocycles was found, which may be interpreted as a "bending" of the corresponding bonds. This "bending" was confirmed by calculations of characteristics of the electron density distribution within the multipole model.
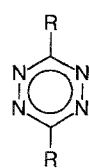
Key words: tetrazines, molecular geometry, quantum-chemical calculations, X-ray structural analysis, electron density distribution.

1,2,4,5-Tetrazine, or *s*-tetrazine (**1**), and its derivatives are rather little studied. These compounds are used in organic synthesis[1]; some derivatives of tetrazines exhibit biological activity.[2] Recently, tetrazines came into use as bridging ligands in the synthesis of conducting macrocyclic complexes (phthalocyanine derivatives of Mn, Fe, Rh, and Ru) (see, for example, Refs. 3 and 4). Polymers based on these complexes exhibit semiconductor properties[3]; the ability to readily transfer electronic effects through the heterocyclic ligand is associated with a number of spectral properties of tetrazines, in particular, with a low energy of the π^* orbitals.[4,5] A low energy of the n → π^* transition in tetrazines causes a deep color of the majority of these compounds and acceptor properties of the heterocycle.[5,6] Note that tetrazines have been studied by different spectroscopic[5-9] and quantum-chemical methods[10-14] as representatives of a series of aromatic azines, with the aim of elucidating their electronic structures, the character of electron delocalization, and the degree of aromaticity of heterocycles in detail.

X-ray structural data are available for *s*-tetrazine (**1**, photographic method[15]) and for some symmetrical 3,6-disubstituted derivatives (**2—6**).[16-19]

R	Compound	**1**	**2**	**3**	**4**	**5**	**6**
	R	H	Me	Ph	NH_2	N◁	OMe
	References	15	16	17	18	19	19

In these works, the planar structure of the heterocycle and the lengths of the N—C and N—N bonds (~1.34 Å and ~1.32 Å, respectively) intermediate between those of double and single bonds were noted, which is a structural evidence for electron delocalization in the cycle. When bisaziridine (**5**) and dimethoxyl (**6**) derivatives were studied, the conclusion was also made[19] about a strong acceptor character of the *s*-tetrazine nucleus, which manifests itself in shortening of exocyclic C—N and C—O bonds (to 1.385 and 1.328 Å, respectively) compared to the normal single bonds.

The simple crystal and molecular structures of tetrazines provide a possibility of studying the electron density distribution in crystals of these compounds by the X-ray diffraction method. The corresponding studies make it possible to reconstruct the electron density distribution function $\rho(r)$ in molecules and crystals with a high degree of accuracy and to formulate the fundamental concepts concerning the nature of chemical bonds in these compounds in terms of experimentally determined features of the function $\rho(r)$.[20-22] For this purpose in this work, the precision low-temperature (150 and 120 K) X-ray structural study of crystals of 3,6-dimethoxy-*s*-tetrazine (**6**) and 3-phenyl-*s*-tetrazine (**7**) was carried out, and electron density maps were calculated; to compare experimental and theoretical data, quantum-chemical and conformational calculations for molecules **1**, **6**, and **7** in the free state were performed. This work was undertaken as part of continuing systematic studies of characteristic features of electron distribution

in nitrogen-containing heterocycles (see Refs. 23 and 24).

Experimental

Single crystals of compounds **6** and **7** were obtained as thin plates by slow crystallization from ethanol. X-ray diffraction studies were performed at 150 K (**6**) and 120 K (**7**) on automated four-circle Syntex P2₁ and Siemens P3/PC diffractometers (Mo-Kα radiation, graphite monochromator, θ/2θ scanning technique, 2θ < 85°, sinθ/λ < 0.95 Å⁻¹).

Crystals of **6** are orthorhombic, at 150 K: a = 6.654(1), b = 13.034(2), c = 6.949(1) Å, V = 602.7(2) Å³, Z = 4, d_{calc} = 1.567 g cm⁻³, space group *Pbca*.

Crystals of **7** are monoclinic, at 120 K: a = 8.101(1), b = 18.718(3), c = 5.499(1) Å, β = 119.87(2)°, V = 723.1(7) Å³, Z = 4, d_{calc} = 1.453 g cm⁻³, space group *C2/c*. In crystals, molecules **6** and **7** occupy the special positions (inversion centers (**6**) and twofold axes (**7**)).

Of a total number of measured (8037 for **6** and 8795 for **7**) reflections (data sets were collected within a hemisphere in reciprocal space, the R_{int} factor for intensities of equivalent reflections were 0.032 and 0.040 for **6** and **7**, respectively), 886 and 986 independent observed reflections with $I > 4\sigma(I)$ were used in subsequent calculations and refinement. The structures were solved by the direct method and were refined by the least-squares method with anisotropic thermal parameters for nonhydrogen atoms and isotropic thermal parameters for hydrogen atoms. Absorption corrections were applied using experimental curves of ψ scanning; extinction was ignored because it is negligible. With the aim of obtaining accurate values of positional and thermal parameters of nonhydrogen atoms the structures were refined with the use of the Dunitz—Seiler's weighting scheme (a quasi-high-order refinement) with the

coefficients B = 6.0,[25] the parameters of H atoms being fixed. The results of the refinement are as follows: R = 0.034, R_w = 0.034, GOF = 1.305 for **6**; R = 0.048, R_w = 0.049, GOF = 1.94 for **7**. The atomic coordinates and isotropic equivalent temperature factors that correspond to this refinement are given in Table 1; the molecular structures and atomic numbering schemes are shown in Fig. 1; the bond lengths and bond angles are listed in Table 2.

Table 1. Atomic coordinates (×10⁴, for H ×10³) and isotropic equivalent (isotropic for H) temperature factors in the structures of **6** and **7**

Atom	x	y	z	$U \cdot 10^3/\text{Å}^2$
		Structure **6**		
O	1556(1)	4328(1)	1235(1)	21(1)
N(1)	4550(1)	3997(1)	−335(1)	17(1)
N(2)	6295(1)	4357(1)	−932(1)	17(1)
C(1)	3326(1)	4651(1)	573(1)	15(1)
C(2)	937(2)	3303(1)	687(1)	21(1)
H(1)	−39(3)	323(1)	120(3)	37(4)
H(2)	181(3)	282(1)	125(2)	29(4)
H(3)	87(3)	329(2)	−66(3)	38(4)
		Structure **7**		
N(1)	5870(1)	4069(1)	1283(2)	26(1)
N(2)	5878(1)	3361(1)	1283(2)	24(1)
C(1)	5000	4392(1)	2500	29(1)
C(2)	5000	3026(1)	2500	19(1)
C(3)	5000	2235(1)	2500	20(1)
C(4)	5942(1)	1860(1)	1349(2)	23(1)
C(5)	5948(2)	1115(1)	1366(2)	26(1)
C(6)	5000	745(1)	2500	26(1)
H(1)*	500	489(1)	250	42(5)
H(4)	665(2)	210(1)	53(3)	39(3)
H(5)	669(2)	85(1)	55(3)	40(4)
H(6)	500	22(1)	250	36(4)

* Numbering of H atoms is assigned to the corresponding C atoms.

Table 2. Bond lengths and bond angles in the structures of **6** and **7**

| Bond	$d/\text{Å}$	Angle	φ/deg
		Structure **6**	
C(1)—O	1.333(1)	C(1)—O—C(2)	116.9(1)
C(2)—O	1.448(1)	O—C(1)—N(1)	119.9(1)
C(1)—N(1)	1.337(1)	O—C(1)—N(2a)	114.0(1)
N(1)—N(2)	1.320(1)	N(1)—C(1)—N(2a)	126.0(1)
C(1)—N(2a)	1.341(1)	C(1)—N(1)—N(2)	117.2(1)
		N(1)—N(2)—C(1a)	116.8(1)
		Structure **7**	
N(1)—C(1)	1.334(1)	N(1)—C(1)—N(1a)	126.1(1)
N(1)—N(2)	1.324(1)	C(1)—N(1)—N(2)	117.2(1)
N(2)—C(2)	1.349(1)	N(1)—N(2)—C(2)	117.5(1)
C(2)—C(3)	1.481(2)	N(2)—C(2)—N(2a)	124.6(1)
C(3)—C(4)	1.399(1)	N(2)—C(2)—C(3)	117.7(1)
C(4)—C(5)	1.395(1)	C(2)—C(3)—C(4)	120.1(1)
C(5)—C(6)	1.391(1)	C(4)—C(3)—C(4a)	119.8(1)
		C(3)—C(4)—C(5)	119.9(1)
		C(4)—C(5)—C(6)	120.0(1)
		C(5)—C(6)—C(5a)	120.2(1)
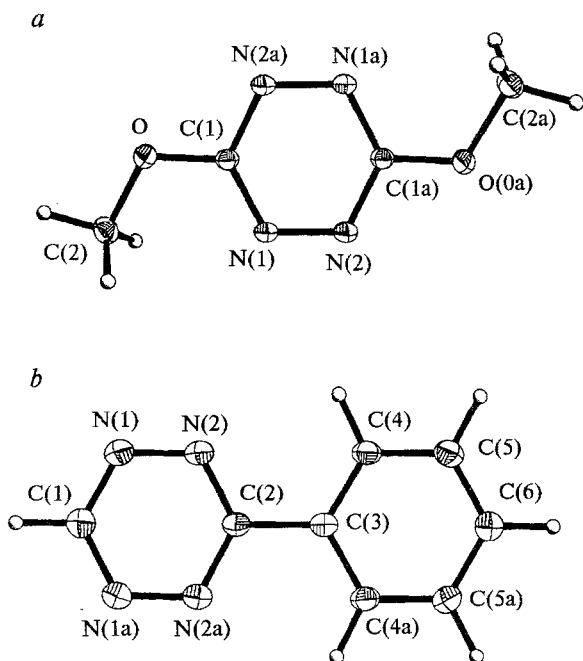
Fig. 1. Overall views of molecules **6** (*a*) and **7** (*b*) and the atomic numbering scheme; nonhydrogen atoms are represented by thermal ellipsoids (p = 50 %).

The deformation electron density maps were calculated by the "X-X" method (see, for example, Refs. 20 and 21) with the use of the results of the high-order refinement based on 456 and 418 reflections with $\sin\theta/\lambda > 0.65$ Å^{-1} for a model of a "promolecule". The results of this refinement are as follows: $R = 0.029$, $R_w = 0.026$, GOF $= 0.95$ for **6**; $R = 0.038$, $R_w = 0.038$, GOF $= 1.36$ for **7**. Note that although the high-order refinement gave lower values of R factors, errors in determining structural parameters were twice as large as those obtained by the high-order refinement according to the scheme reported in Ref. 25, which is associated with a smaller number of reflections used in the least-squares refinement.

All crystallographic calculations were performed on an IBM PC/AT computer using the SHELXTL PLUS program package. The geometries of molecules **1**, **6**, and **7** in the free state were calculated by the molecular mechanics method using the MM3 program[26]; quantum-chemical calculations with optimization of the geometry in the RHF/6-31G* and MP2/6-31G** approximations were carried out on a RISC 6000 computer (Laboratory of Prof. N. L. Allinger, University of Georgia, Athens, USA) using the GAUSSIAN-92 program package.

Results and Discussion

The geometric parameters of molecules **6** and **7** in the crystals have the expected values. In the structure of **6**, the atoms of the heterocycle and the adjacent O atoms are coplanar within 0.006 Å, whereas the methyl C atoms deviate from this plane by ±0.167 Å; the N(1)—C(1)—O—C(2) torsion angle is −8.6°. Of the characteristic features of the molecular geometry of **6**, the inequality of the exocyclic N(1)—C(1)—O and N(2a)—C(1)—O bond angles (119.9(1) and 114.0(1)°, respectively) should be noted; apparently, this difference is associated with the repulsion between the N(1) and methyl C(2) atoms; the N(1)...C(2) nonbonded distance is 2.663 Å. The methyl H atoms are oriented so that the intramolecular distances between the N(1) atom of the heterocycle and the H(2) and H(3) atoms of this group are equal (2.65 Å), whereas the H(1) atom lies close to the plane of the heterocycle and deviates from this plane by 0.20 Å; the C(1)—O—C(2)—H(1) torsion angle is −175°. As noted in Ref. 19, the C(1)—O bond in **6** is substantially shortened (to 1.333(1) Å), which is indicative of its increased multiplicity.

Molecule **7** is planar; all its atoms, including hydrogen atoms, are coplanar within 0.016 Å; the N(2)—C(2)—C(3)—C(4) torsion angle is 2.1°. Note the inequality of the C(1)—N(1) and C(2)—N(2) bond lengths (1.334(1) and 1.349(1) Å, respectively) and of the endocyclic *ipso* angles at the C(1) and C(2) atoms (126.1(1) and 124.6(1)°, respectively). This may be a result of the electronic effect of the Ph substituent as well as (apparently, to a greater extent) a result of steric interaction between closely located N(2) and H(4) atoms. The intramolecular nonbonded N(2)...H(4) distance in **7** is 2.53 Å. Note that the C(3)—C(4)—H(4) bond angle (123.2(9)°) is larger than the C(5)—C(4)—H(4) bond angle (116.9(9)°).

It is of interest to compare the geometries of molecules **6** and **7** and unsubstituted tetrazine **1** both in the crystal and in the free state (based on conformational and quantum-chemical calculations). Table 3 gives the principal geometric characteristics of the tetrazine fragments of molecules **1**, **6**, and **7** obtained by X-ray structural analysis (for the crystal of **1**, these data were obtained in the study of the electron distribution in *s*-tetrazine at 120 K[24]; the results of this study will be published elsewhere), as well as those obtained by conformational calculations by the molecular mechanics method (MM3) and by quantum-chemical calculations of the optimized geometry in the RHF/6-31G* and MP2/6-31G** approximations. As is evident form Table 3, the geometry of the tetrazine fragment changes only slightly in going from unsubstituted tetrazine **1** to its derivatives **6** and **7**. In this series of compounds, only a slight elongation of the C—N bonds and a decrease in the *ipso* N—C—N angle in molecule **7** on the side of the Ph substituent are observed. Calculations with the use of the MM3 program reproduce well experimental geometry of the heterocycle (an average discrepancy between the experimental and calculated bond lengths and bond angles are 0.004 Å and 0.4°, respectively).

A discrepancy between the results of quantum-chemical calculations and experimental data are larger, some lengths of the same bonds calculated by the RHF and MP2 methods differ rather substantially. In particular, the RHF method underestimated the N—N bond lengths (and the C—N bond lengths to a lesser degree), which is, apparently, because the electronic correlation was ignored. The MP2 calculations gave a better agreement with the experimental geometry. Note that an analogous trend was observed also when the geometries of *s*-tetrazine and its 1,2,3,4- and 1,2,3,5-isomers were calculated with different basis sets.[27] Nevertheless, quantum-chemical calculations adequately reproduce the general trend of changes in molecular geometry in a series of compounds under consideration.

Table 3 gives also the results of X-ray structural analysis obtained when the structural parameters were refined with the use of not only all reflection but of high-order reflections as well ($\sin\theta/\lambda > 0.65$ Å^{-1} for **6** and **7** and $\sin\theta/\lambda > 0.85$ Å^{-1} for **1**). It is remarkable that the N—N bond obtained from the high-order refinement is shorter, for structures **1** and **7** this difference (0.006—0.007 Å) being rather significant. This difference becomes even larger if the results of the high-order and low-order refinements are compared when the set of reflections used in the least-squares procedure is limited "from above" by $(\sin\theta/\lambda)_{max} = 0.6$ Å^{-1}, which is usually the upper limit of X-ray diffraction data in conventional experiments ($2\theta = 50°$ for Mo radiation). In the case of the low-order refinement, the N—N bond lengths are 1.329(1), 1.325(1), and 1.328(1) Å for structures **1**, **6**, and **7**, respectively. Therefore, the discrepancy between the N—N bond lengths obtained from the low-order and high-order refinements was 0.010(1) Å, which is an

Table 3. Principal geometric parameters of tetrazine heterocycles **1**, **6**, and **7** based on X-ray structural data and conformational (MM3) and quantum-chemical (RHF and MP2) calculations

Parameter	Method of determination	1	6		7	
d(N—N)/Å	X-ray structural analysis	1.325(1)	1.320(1)		1.324(1)	
	X-ray structural analysis (high-order refinement)	1.319(1)	1.317(2)		1.317(2)	
	MM3	1.318	1.325		1.323	
	RHF	1.291	1.287		1.287	
	MP2	1.341	1.335		—	
d(C—N)/Å	X-ray structural analysis	1.332(1)	1.337(1)	1.341(1)	1.334(1)	1.349(1)
	X-ray structural analysis (high-order refinement)	1.334(1)	1.338(1)	1.342(1)	1.333(2)	1.351(2)
	MM3	1.336	1.345	1.346	1.337	1.349
	RHF	1.318	1.317	1.318	1.317	1.327
	MP2	1.345	1.349	1.350	—	
φ(N—C—N)/deg	X-ray structural analysis	126.0(1)	126.0(1)		126.1(2)	124.6
	X-ray structural analysis (high-order refinement)	125.7(1)	125.7(1)		125.6(2)	124.0
	MM3	127.2	125.7		126.9	123.9
	RHF	125.1	124.1		124.4	123.0
	MP2	127.2	126.5		—	
φ(C—N—N)/deg	X-ray structural analysis	116.9(1)	117.2(1)	116.8(1)	117.2(1)	117.5(1)
	X-ray structural analysis (high-order refinement)	117.0(1)	117.4(1)	116.9(1)	117.5(2)	117.7(2)
	MM3	116.4	117.1		116.3	118.2
	RHF	117.5	118.5		117.8	118.5
	MP2	116.4	117.3	116.1	—	

order of magnitude larger than the experimental error. In accordance with the changes in bond lengths, the N—C—N bond angles obtained from the above-mentioned refinements were slightly increased (by 0.5°) in all three structures.

This can be accounted for by the fact that when X-ray diffraction data are used, the atomic positions are determined not by the coordinates of atomic nuclei (as in the case of neutron diffraction studies) but by the coordinates of centroids of atomic electron densities, and in the general case these two values do not coincide. In particular, the presence of hybridized atomic orbitals of the lone electron pairs of the N and O atoms and atoms of other light elements may result in an effective shift of the centroids of the atomic electron density determined from the X-ray structural analysis toward the lone electron pairs of these atoms. Therefore, the N—N bond lengths in the structures under study, which were obtained by the low-order refinement, were overestimated by almost 0.01 Å. In the general case, the interpretation of fine details of molecular geometries of organic compounds based on the data obtained by the low-order refinement (or, for example, obtained in the experiments performed with the use of Cu radiation, because in this case the maximum possible value of $\sin\theta/\lambda$ is 0.65 Å^{-1}) should be considered with caution. To the contrary, when the results of the high-order refinement are used, the contribution of lone electron

pairs to X-ray scattering substantially decreases, and atomic coordinates (centroids of the electron density in X-ray structural analysis) virtually coincide with the position of atomic nuclei, *i.e.*, the bond lengths correspond to the true internuclear distances.

Let us consider the characteristic features of the deformation electron density distribution maps in molecules **6** and **7**; Figs. 2 and 3 show the deformation electron density maps in the plane of the heterocycle. By definition,[20–22] these maps demonstrate the redistribution of the electron density of a superposition of noninteracting atoms (a promolecule) upon formation of chemical bonds. What is the deformation electron density maps shown in the above-mentioned figures have in common is the presence of pronounced maxima of the deformation electron density in all chemical bonds as well as in the planes of the cycles near the atomic nuclei of N atoms, where their lone electron pairs are located. The character of the arrangement of peaks of the positive deformation electron density about the C and N atoms is close to planar-trigonal, which corresponds to sp^2 hybridization of their atomic orbitals including atomic orbitals of the lone electron pairs of N atoms. In addition, the peak in the region of the lone electron pair of the O atom with the height of 0.20 $e\cdot$ Å^{-3} is observed in Fig. 2; this peak virtually coalesces with two other maxima of the deformation electron density in the C—O and C—Me bonds.
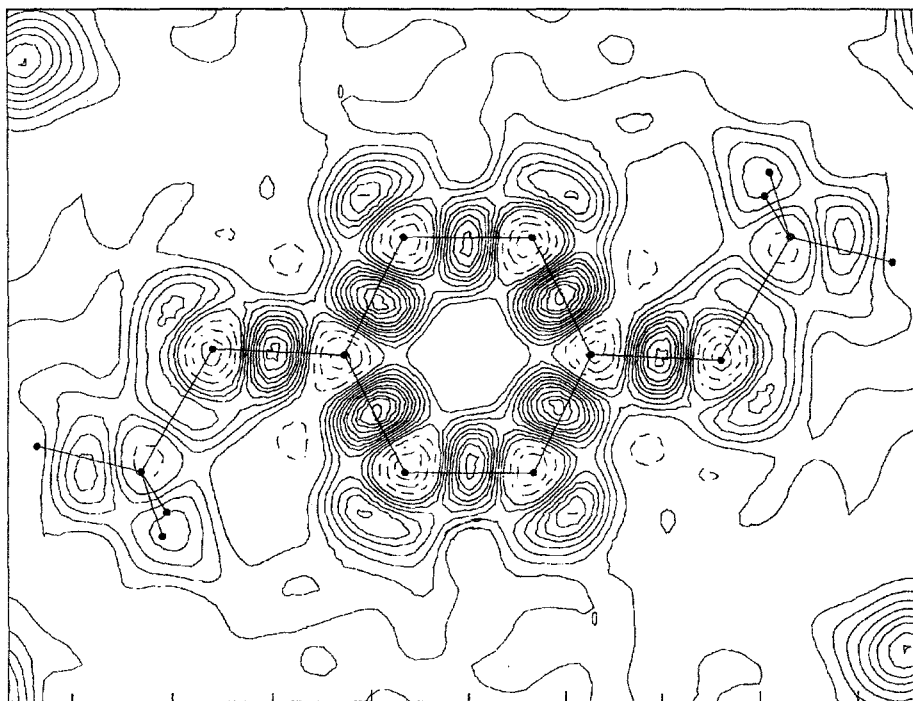
Fig. 2. Section of the deformation electron density in the plane of molecule **6**; contour intervals are $0.05\ e \cdot Å^{-3}$. Negative contours are denoted by dashed lines; contour intervals are $0.1\ e \cdot Å^{-3}$.

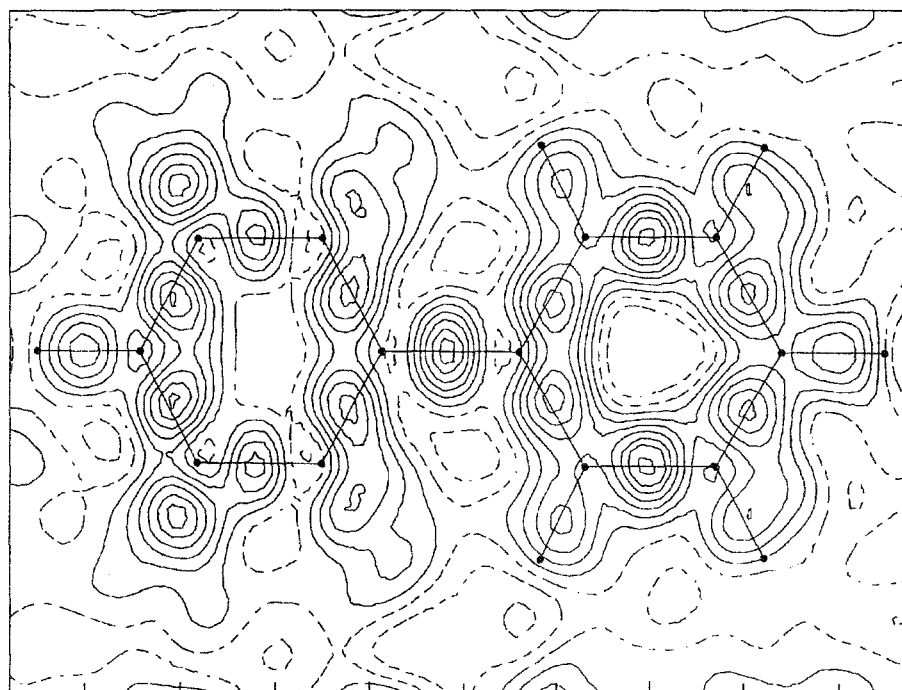**Fig. 3.** Section of deformation electron density in the plane of molecule **7**; contour intervals are $0.05\ e \cdot Å^{-3}$.

The heights of the peaks of the deformation electron density in the regions of the nitrogen lone electron pairs in structure **6** are virtually the same $(0.30—0.35\ e \cdot Å^{-3})$; however, in **7**, the peaks corresponding to the lone electron pairs of the $N(2)$ and $N(2a)$ atoms near the benzene cycle are more diffused and less pronounced than the analogous maxima for the $N(1)$ and $N(1a)$ atoms. The maximum values of the deformation electron density in

the regions of the lone electron pairs of the N(1) and N(2) atoms are 0.25 and 0.15 $e \cdot$ Å^{-3}, respectively. This feature of electron distribution (see Fig. 3) may be associated with a possible intramolecular interaction of the lone electron pairs of the N(2), N(2a) and H(4), H(4a) atoms located in the plane of the molecule. The possibility of such interaction follows from a characteristic distortion of the geometry of the heterocycle in the structure of 7 (see above).

The characteristic features of the sections of the deformation electron density passing through the C(1)—O bond and the O atom perpendicular to the plane of molecule 6 (Fig. 4, *a,b*) are remarkable. As mentioned above, the C(1)—O bond in the structure of 6 is shortened, which is, apparently, caused by its increased multiplicity. The peak of the deformation electron density in this bond has a pronounced π component (see Fig. 4, *a*), *i.e.*, this peak is extended along the axis orthogonal to the C(1)—O bond and to the plane of the molecule. The section of the deformation electron density passing through the O atom along the bisector of the C(1)—O—C(2) angle is shown in Fig. 4, *b*; points *1* and *2* (at a distance of 1 Å from the O atom) are given for clarity, and they correspond to the "ideal" orientation of two lone electron pairs of the O atom with sp^3 hybridization. It is seen from this figure that the maxima of the peaks of two lone electron pairs of this atom (A and B) are poorly resolved and almost coalesce, which is typical of the O atoms of ether groups (see, for example, Ref. 22). As a whole, the patterns of the deformation electron densities in Figs. 2 and 4 are indicative of a substantial electron delocalization from the lone electron pair of the O atom to the C(1)—O bond.

In our opinion, the most remarkable feature of the deformation electron density maps in Figs. 2 and 3 is the shift of the maxima of the deformation electron density from all N—N and C—N bonds in 6, as well as from the C(1)—N(1) and C(1)—N(1a) bonds in 7 inward (toward the centers of the heterocycles), which may be interpreted as the "bending" of these bonds. These shifts are small and are equal to 0.08—0.11 Å. Nevertheless, these shifts are clearly reproduced in all deformation electron density maps calculated with the use of different models of the promolecule (the quasi-high-order refinement or modifications of the high-order refinement with different lower limits for sinθ/λ).

An alternative explanation of the shifts observed could lie in the fact that the least-squares refinement of structures based on the total set of reflections gives atomic coordinates of the N atoms shifted toward their lone electron pairs because of a substantial contribution of these lone electron pairs to X-ray scattering (see above; this effect causes an elongation of the N—N bonds upon refinement of structures with the use of the low-order data). In this case, the "bending" of bonds as an artifact should disappear when maps are calculated with the use of the models from the high-order refinement. However, in the structures of 6 and 7, the

"bendings" are still observed when the models from the high-order refinement are used, which, apparently, reflects the real feature of the electron density distribution in tetrazine heterocycles.

It is known that formation of bent bonds is typical of carbocyclic molecules containing strained small cycles (derivatives of cyclopropane and cyclobutane) or three-dimensional cages (derivatives of tetrahedrane, cubane, and prismane). In the deformation electron density maps of these molecules in the planes of small cycles, the corresponding maxima are usually shifted (up to 0.3—0.4 Å) from the lines of the C—C bonds of the cycle outward.[28,29] Therefore, the "bending" of bonds inside the tetrazine heterocycles observed in this work is somewhat unexpected because such "bending" has never been experimentally observed for organic compounds.

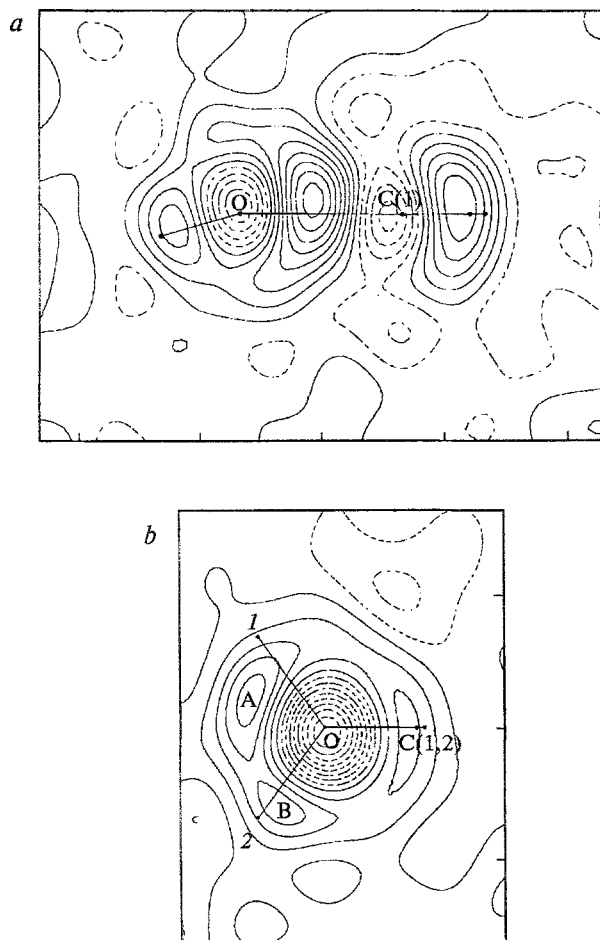The "bending" of the N—N and C—N bonds in the structures of 6 and 7 is attributable to the "stereochemical

Fig. 4. Sections of the deformation electron density passing through the C(1)—O bond perpendicular to the plane of molecule 6 (*a*) and through the O atom in the bisecting plane (*b*). Points *1* and *2* in Fig. *b* correspond to the "ideal" orientation of the lone electron pair of the O atom with a *1*—O—*2* angle of 109°. Contour intervals are 0.05 $e \cdot$ Å^{-3}.

activity" of the powerful lone electron pairs of the N atoms, which are located in the plane of the heterocycles and which force the electron density from the N—N and C—N bonds of the heterocycles inward (electrostatic repulsion). It is remarkable that in molecule 7, in which the electron density of the lone electron pairs of the N(2) and N(2a) atoms is decreased, the maxima of the deformation electron density in both N—N bonds (N(2)—C(2) and N(2a)—C(2)) are not shifted; instead, the peaks of the deformation electron density of the peripheral N(1)—C(1) and N(1)—C(1a) bonds and the C(3)—C(4) and C(3)—C(4a) bonds of the benzene ring appear to be shifted.

The observed characteristic features of the deformation electron density for molecules 6 and 7 (and for 1) were confirmed by quantum-chemical calculations (the 6-31G** basis) of electronic structures of a series of aromatic azines, including s-tetrazine.[14] In this work, the quantum-topological approach of R. Bader[30] was used for the description of bonds in a series of compounds under consideration. According to this approach, the chemical bond is determined not as the shortest distance between atoms but as a bond path along which the total electron density in the region between these atoms has the maximum value compared to those of other possible paths (not necessarily straight lines) connecting atomic nuclei in the equilibrium molecular structure. This path, which is unambiguously determined[30] as a line of gradient of $\rho(r)$, is characterized by the presence of the so-called critical point r_c, in which the minimum electron density along the bond line and the maximum density in two other perpendicular directions correspond to the function $\rho(r_c)$. The critical point (of the (3, −1) type according to the classification given in Ref. 30), in respect of a number of nonzero eigenvalues of the Hessian matrix and the algebraic sum of its signs, is the saddle point of the function $\rho(r)$ in the internuclear space of chemically bonded atoms. The position of this point with respect to the line connecting atomic nuclei determines the "bending" of the bond.

An application of this approach for describing "bent" bonds in small cycles has been discussed in the literature.[31,32] In the general case, the length of the chemical bond, which is determined as the shortest internuclear distance, and the bond path do not coincide; it is for small cycles that the largest discrepancy between these characteristics is observed. According to calculations on azines,[14] the N—N bonds and, to a smaller extent, the C—N bonds are also "bent" (inside the cycles), whereas in the pyridine—pyrazine—pyrimidine—pyridazine—s-triazine—s-tetrazine series, the largest "bend" of bonds is found for the N—N bonds in pyrazine and s-tetrazine. Therefore, in this work the "bending" of bonds in the tetrazine heterocycles, which has been theoretically predicted previously, was observed experimentally.

An additional information on characteristic features of chemical bonds in tetrazines can be gained from the data obtained from the refinement of the structures

studied within the multipole model,[33] which makes it possible to represent functions of the total and the deformation electron density ($\rho(r)$ and $\Delta\rho(r)$) in the analytical form. According to this model, the aspherical electron density of each atom in the crystal $\rho_{at}(r)$ is represented as the sum of the undeformed Hartree—Fock densities of the core (ρ_{core}) and valence (ρ_{val}) shells and spherical harmonic functions Y_{lm} (multipoles) that describe the deformation of the valence shell upon involvement of the atom in a chemical bond. Electron population coefficients of core and valence shells of atoms (ρ_{core} and ρ_{val}) and populations of multipoles Y_{lm} as well as a number of other parameters of the model were refined based on X-ray diffraction data (see Refs. 20—23, 33 for details).

An analytical representation of the total electron density and deformation electron density within the multipole model allows calculations of charges on atoms in molecules and crystals (as a measure of population of valence shells) and many other electrical properties. In this case, it is possible to calculate maps of the so-called "static" deformation electron density, which is not smeared by the effects of thermal vibrations of atoms. These maps are "clearer", and in these maps, fine details of electron distribution are more pronounced. Figure 5 shows the static deformation electron density map in the plane of molecule 6, which we calculated in the multipole approximation. It is evident that the principal features of the deformation electron density maps shown in Figs. 2 and 5 are similar including the observed shift of the maxima of the deformation electron density from the N—N bonds inside the heterocycle. Note that the ways of calculating the electron distribution maps shown in Fig. 2 (the dynamic deformation electron density represented by the difference Fourier series) and in Fig. 5 (the static deformation electron density calculated directly with the use of the multipole refinement) are substantially different, and, hence, the reproduction of the same characteristic features of the deformation electron density in these maps may be an additional corroboration of the "bending" of the N—N bonds in the tetrazine heterocycle.
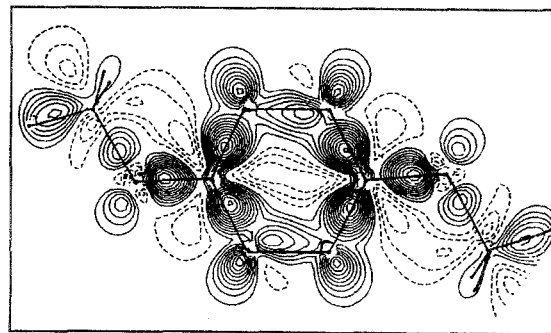

Fig. 5. Map of the static multipole deformation electron density in the plane of molecule 6; contour intervals are 0.1 $e \cdot Å^{-3}$.
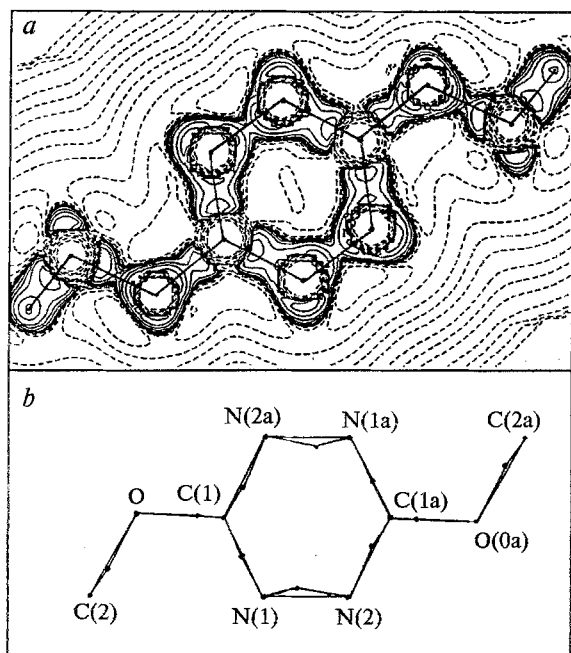
Fig. 6. Map of the Laplacian of the electron density $\nabla^2\rho(r)$ in the plane of molecule **6** (*a*) and the critical points of the type (3, −1) in the bonds of the heterocycle (*b*); solid contours correspond to the levels of negatives values of $\nabla^2\rho(r)$ (the logarithmic scale).

Currently, the experimental determination of coordinates of the saddle points (the critical points of the (3, −1) type, see above) of the function $\rho(r)$ and of the bond path is carried out within the multipole analysis of X-ray diffraction data upon topological analysis of the function $\rho(r)$, in particular, of its Laplacian $\nabla^2\rho(r)$. According to definition,[30] the values $-\nabla^2\rho(r) > 0$ correspond to the regions of local concentration of $\rho(r)$, whereas in the region of local rarefaction of $\rho(r)$, $-\nabla^2\rho(r) < 0$. It was demonstrated (see, for example, Refs. 20—22, 30) that the negative values of the function $\nabla^2\rho(r)$ in the corresponding maps (two-dimensional sections) correspond to those regions of the space in molecules or crystals, in which the contribution of the local potential energy prevails, *i.e.*, correspond to the regions of chemical bonding. These maps serve as a useful supplement of the deformation electron density maps, because these maps are not difference maps, *i.e.*, they are not model-dependent. The critical point of the bond r_c is determined by the equation $\nabla[\nabla^2\rho(r)] = 0$. Note that examples of such topological analysis of the characteristics of the electron density in the region of the chemical bond with the use of X-ray diffraction data are scarce as yet.[34]

In this work, the values of the function $\nabla^2\rho(r)$ and positions of the critical points (3, −1) in the bonds of the heterocycle were calculated for the structure of **6** in the multipole approximation using the XDPROP program.[35] Figure 6 shows the section of the function $-\nabla^2\rho(r)$ in the plane of the heterocycle and gives posi-

tions of the critical points with respect to the lines connecting atomic nuclei. It is evident that negative values of this function correspond to the maxima of the deformation electron density (in Figs. 2 and 5) located both between atomic nuclei and in the regions of the lone electron pairs of the N and O atoms. Note also a slight shift inside the cycle of the saddle points of the N—N bonds. Coordinates of the critical points of the (3, −1) type, the positions of which are shown in the lower part of Fig. 6, agree well with the characteristic features of the deformation electron density maps discussed above and confirm the unusual "bending" of the bonds in the tetrazine heterocycle.

References

1. D. T. Hurst, *Prog. Heterocycl. Chem.*, 1992, **4**, 204.
2. M. Jag and K. Sangeeta, *Ind. J. Chem., Sect. B*, 1994, **33B**(2), 196.
3. S. Hayashida and M. Hanack, *Synth. Met.*, 1992, **52**, 241.
4. J. Poppe, M. Moscherosch, and M. Kaim, *Inorg. Chem.*, 1993, **32**, 2640.
5. R. Gleiter, V. Schehlmann, J. Spanget-Larsen, H. Fischer, and F. A. Neugebauer, *J. Org. Chem.*, 1988, **53**, 5756.
6. G. H. Spencer, Jr., P. C. Cross, and K. Wiberg, *J. Chem. Phys.*, 1961, **35**, 1925.
7. V. A. Job and K. K. Innes, *J. Mol. Spectrosc.*, 1978, **71**, 299.
8. K. K. Innes and D. V. Brumbauch, *Chem. Phys.*, 1981, **59**, 439.
9. D. V. Brumbauch and K. K. Innes, *Chem. Phys.*, 1981, **59**, 413.
10. S. Knuts, O. Vahtas, and H. Aagren, *J. Mol. Struct., THEOCHEM*, 1993, **98**, 249.
11. D. E. Williams and R. R. Weller, *J. Am. Chem. Soc.*, 1983, **105**, 4143.
12. P. Politzer, J. S. Murray, J. M. Seminario, and R. S. Miller, *J. Mol. Struct., THEOCHEM*, 1992, **94**, 155.
13. N. Russo, *Struct. Chem.*, 1992, **3**(3), 163.
14. K. N. Wiberg, D. Nakaji, and C. M. Breneman, *J. Am. Chem. Soc.*, 1989, **111**, 4178.
15. F. Bertinotti, G. Giacomello, and A. M. Liuori, *Acta Crystallogr.*, 1956, **9**, 510.
16. J. C. Huffman, *Cryst. Struct. Commun.*, 1981, **10**, 227.
17. N. A. Ahmed and A. I. Kitaigorodsky, *Acta Crystallogr.*, 1972, **B28**, 739.
18. C. Krieger, H. Fischer, and F. A. Neugebauer, *Acta Crystallogr.*, 1987, **C43**, 1320.
19. C. Krieger, H. Fischer, F. A. Neugebauer, F. Guckel, and D. Schweitzer, *Acta Crystallogr.*, 1987, **C43**, 1412.
20. P. Coppens, *Ann. Rev. Phys. Chem.*, 1992, **43**, 663.
21. *The Application of Charge Density Research to Chemistry and Drug Design*, Ed. G. A. Jeffrey and J. F. Piniella, NATO ASI Series, Ser. B: Physics, **250**, 409 pp.

22. V. G. Tsirel'son, *Khimicheskaya svyaz' i teplovoe dvizhenie atomov v kristallakh* [*Chemical Bonds and Thermal Motion of Atoms in Crystals*], in *Itogi Nauki Tekh., Ser.: Kristallokhim.*, 1992, **27**, 268 (in Russian).
23. M. Yu. Antipin and E. A. Kuz'mina, *Izv. Akad. Nauk, Ser. Khim.*, 1995, 495 [*Russ. Chem. Bull.*, 1995, **44**, 478 (Engl. Transl.)].
24. M. Yu. Antipin, Yu. T. Struchkov, and J. Sauer, *Am. Cryst. Ass. Ann. Meeting*, June 26—July 1, Atlanta, 1994, 164.
25. J. D. Dunitz and P. Seiler, *Acta Crystallogr.*, 1973, **B29**, 589.
26. J. C. Tai, L. Yang, and N. L. Allinger, *J. Am. Chem. Soc.*, 1993, **115**, 11906.
27. J. R. Thomas, G. E. Quelch, and H. F. Schaefer III, *J. Org. Chem.*, 1991, **56**, 539.
28. R. Boese, D. Blaser, W. E. Billups, M. M. Haley, A. H. Maulitz, D. L. Mahler, and K. C. P. Vollhardt, *Angew. Chem., Int. Ed. Engl.*, 1994, **33**, 313.

29. H. Irngartinger and T. Oeser, *Acta Crystallogr.*, 1994, **B50**, 459.
30. R. F. W. Bader, *Atoms in Molecules. A Quantum Theory*, Oxford Sci. Publ., Clarendon Press, Oxford, 1990, 438 pp.
31. D. Cremer and E. Kraka, *J. Am. Chem. Soc.*, 1985, **107**, 3800.
32. D. Cremer and E. Kraka, *J. Am. Chem. Soc.*, 1985, **107**, 3811.
33. N. H. Hansen and P. Coppens, *Acta Crystallogr.*, 1978, **A34**, 909.
34. C. Gatti, R. Bianchi, R. Destro, and F. Merati, *J. Mol. Struct., THEOCHEM*, 1992, **255**, 409.
35. S. T. Howard, *XDPRPOP — One-Electron Properties from Multipole Refinement*, Private Communication, 1994.